Aeroelastic Load Evaluation During Tiltrotor Transition Using a Comprehensive Mid-Fidelity Approach

A. Cocco, U. Saetti
University of Maryland, College Park - US
A. Savino
Politecnico di Milano, Milano - Italy

ABSTRACT

This study examines the aeromechanics of tiltrotor conversion maneuvers using a coupled simulation approach, integrating the multibody dynamics code MBDyn with the mid-fidelity aerodynamic code DUST. The analytical model is based on the XV-15 tiltrotor with advanced technology blades. The hover and cruise performances of the model are validated against available test data, ensuring accuracy. A generic tiltrotor control system is developed using a nonlinear dynamic inversion control law to simulate transient conversion maneuvers. The investigation includes time histories of vehicle dynamics, rotor control inputs, rotor flapping, rotor performance, and blade structural loads, providing detailed insights into the behavior of tiltrotor aircraft during conversion.

INTRODUCTION

Tiltrotors, with their ability to take off and land vertically like helicopters and, at the same time, to achieve high speeds up to twice those of helicopters in forward flight when operating like conventional turboprop aircraft, represent one of the few successful examples of advanced vertical lift configurations.

After a long development phase that encompassed few experimental aircraft that successfully made it to flight noticeably, the Transcendental Model 1-G (a tilting rotor concept), which flew about 100 hours without ever completing a full conversion (Ref. 1) and the Bell XV-3 (a tilting rotor configuration), in the 1950s (Ref. 2), and the Bell XV-15 (a tilting rotor/nacelle configuration) in the 1980s (Ref. 1), unlike other less fortunate technology demonstrators, the concept finally proved its soundness with the Bell-Boeing V-22 (a tilting rotor/nacelle configuration) (Ref. 3). Remaining in the military arena, the Bell V-280 Valor (a tilting rotor configuration), after a test campaign started in 2017, at the end of 2022 was selected to replace the UH-60 by the US Army for its Future Long-Range Assault Aircraft (FLRAA) program (Ref. 4). However, with then Bell-Agusta and now Leonardo AW609 (a tilting rotor/nacelle configuration) (Ref. 5) about to become operational after a long and thorough development (Ref. 6), the tiltrotor design appears to be mature enough also to enter the civil air transport market (Ref. 7).

Nevertheless, tiltrotor design remains a rather challenging engineering task, considering the various operating conditions and multipurpose missions expected to be accomplished by this complex type of aircraft. In particular, during the transition maneuver, the rotors are tilted 90 degrees in less than one minute, drastically changing the load components acting on the aircraft: at low speed, most of the weight is carried by the two rotors, while at high speed the rotors provide propulsion and the aircraft's weight is balanced by the wing.

Due to the cost of high-fidelity computational fluid dynamics (CFD), most of the computational research on tiltrotor aircraft has focused on the aircraft in steady or quasi-steady configurations. In (Ref. 8) Tran *et al.* made the first effort towards the simulation of a complete conversion maneuver using a coupled approach between RCAS (Ref. 9) and Helios (Ref. 10). However, this simulation is extremely expensive: on a 1000-core machine, it requires 288 days to be completed. To make the simulation more feasible, in (Ref. 8), the authors used an immersed boundary method to simulate the maneuver: in this way, they could abate the simulation cost by 52 times.

To further reduce the computational time, a viable solution is coupling mid-fidelity aerodynamic codes based on the viscous vortex particle method and multibody comprehensive codes. In 2021, Savino et al. (Ref. 11) coupled the mid-fidelity aerodynamic code DUST (Ref. 12) and MBDyn (Ref. 13) and successfully simulate a rolling maneuver of a complete tiltrotor. The coupled tool has been then used to evaluate the aeroelastic loads in airplane mode (Ref. 14) and whirl flutter stability boundaries (Ref. 15). The ability of DUST to predict discrete

trim conditions in the transition corridor has been previously assessed in (Ref. 16). However, although the predictions in this work were already satisfactory, they were made with an outdated version of DUST, and the structural dynamics of the aircraft were neglected entirely.

This work aims to simulate a complete transition of the XV-15 tiltrotor equipped with advanced technology blades (ATB) using the coupled tool MBDyn-DUST. The work is organized as follows: in the first part, the software tools will be described, particularly the latest update on the mid-fidelity solver DUST. Then, The XV-15 aeroelastic model is described and validated in hover and airplane mode configuration in the second part. In the third part, the control law used for the simulation is presented, and finally, the conversion maneuver is described.

SOFTWARE TOOLS

To obtain an aeroelastic solver with a good balance between the quality of the results and computational cost, the coupling between DUST (Ref. 12) and MBDyn (Ref. 13) is exploited.

MBDyn[1] is a free general-purpose multibody solver. MBDyn automatically writes and solves the equations of motion of a system of entities possessing degrees of freedom (nodes) connected through algebraic constraints and subjected to internal and external loads. The nodes that describe the kinematics of the structural problem can be connected either by elastic/viscoelastic internal forces namely lumped structural components (Ref. 17) and beams (Ref. 18), shells (Ref. 19), and Component Mode Synthesis (CMS) elements (Ref. 20)), with a variety of viscoelastic constitutive laws, or by kinematic constraints. Simple aerodynamics can be modeled by built-in elements that exploit the 2D strip theory model by look-up tables of the aerodynamic coefficients and classical rotor inflow models based on momentum theory.

DUST[2] is a free and open-source code for aerodynamic analysis licensed under MIT. It can handle different levels of fidelity, such as thick or thin surfaces, vortex lattices, or lifting line elements. It also has a vortex particle method for wake modeling that can capture the free-vorticity flow field, which is useful for simulating configurations with strong aerodynamic interactions. In the past year, several improvements have been made to DUST to better capture the loads on the surface panel elements and to improve the physics representation of the particle wake.

Communications between the two solvers are managed by preCICE (Precise Code Interaction Coupling Environment) (Ref. 21), a coupling library for partitioned multi-physics simulations, originally developed for fluid-structure interaction and conjugate heat transfer simulations. The interface between structural and aerodynamic grids is obtained as a weighted average of the distance between the nodes of the two grids. It is used for motion interpolation and consistent force and moment reduction.

The details about the coupling between DUST and MBDyn, with the relative validations, are described in (Ref. 11) in which the flutter speed of the Goland's wing (Ref. 22) has been verified against other analytical tools.

Reformulated Vortex Particle Method

The original `DUST` Implementation is based on the classical VPM formulation, which assumes no evolution of the vortex core sizes in time, *i.e.*, $\dot{\sigma} = 0$. `FlowVPM` (Ref. 23) introduces the so-called reformulated Vortex Particle Method (rVPM), which enforces both the conservation of mass within vortex tubes and of angular momentum of spherical particles within the flow by modifying the particle strength vector differential equation with a proper correction on the vortex-stretching term and by adding a differential equation for the evolution of the smoothing radius σ in time.

Alvarez proposes a generalized form of the VPM governing equations as a function of the parameters f and g, whose values can lead both to the classical ($f = g = 0$) and reformulated ($f = 0\, g = \frac{1}{5}$) formulations. The ordinary differential equations of the reformulated vortex particle method are reported:

$$\frac{d}{dt}\boldsymbol{x}^p = \boldsymbol{u}^h_\sigma(\boldsymbol{x}^p)$$

$$\frac{d}{dt}\boldsymbol{\alpha}^p = (\boldsymbol{\alpha}^p \cdot \nabla)\boldsymbol{u}^h_\sigma(\boldsymbol{x}^p) - \frac{g+f}{\frac{1}{3}+f}\left[(\boldsymbol{\alpha}^p \cdot \nabla)\boldsymbol{u}^h_\sigma(\boldsymbol{x}^p)\cdot\hat{\boldsymbol{\alpha}}^p\right]\hat{\boldsymbol{\alpha}}^p + \\ + 105\nu\frac{\sigma^4}{(\|\boldsymbol{x}^p - \boldsymbol{x}^q\|^2 + \sigma^2)^{\frac{9}{2}}}(vol^p\boldsymbol{\alpha}^q - vol^q\boldsymbol{\alpha}^p)$$

$$\frac{d}{dt}\sigma^p = -\frac{g+f}{1+3f}\frac{\sigma^p}{\|\boldsymbol{\alpha}^p\|}\left[(\boldsymbol{\alpha}^p \cdot \nabla)\boldsymbol{u}^h_\sigma(\boldsymbol{x}^p)\right]\cdot\hat{\boldsymbol{\alpha}}^p$$

The differential equation for σ^p does not require any additional computation since it only depends on the vortex stretching term, which is necessarily calculated in every VPM formulation. It can be observed that the new version of the particle strength equation involves an additional term with respect to the classical formulation, only affecting the stretching component parallel to $\boldsymbol{\alpha}^p$. Hence, all VPM formulations lead to the same turning components acting on the particle strength vector. Conversely, the rVPM ($f = 0\ , g = \frac{1}{5}$) features a 3/5 reduction in the $\frac{d}{dt}\boldsymbol{\alpha}^p$ component parallel to $\boldsymbol{\alpha}^p$ with respect to the cVPM, resulting in a milder rate of change of particle magnitudes in time, in turn considerably increasing the numerical stability of the code. Different from `FlowVPM`, where the viscous effects are modeled using the Core Spreading (CS) algorithm, in `DUST`, these effects are modeled through the Particle Strength Exchange scheme (PSE). The scheme is based

[1] https://public.gitlab.polimi.it/DAER/mbdyn
[2] https://public.gitlab.polimi.it/DAER/dust

on the idea of directly acting on the particles' strength vector $\boldsymbol{\alpha}^p(t)$ through an exchange with neighboring particles instead of modifying their position or core size. The key idea of the method is the substitution of the diffusion operator $\nabla^2\boldsymbol{\omega}$ by an integral approximation as follows:

$$\nabla^2_\sigma \boldsymbol{\omega}(\boldsymbol{x}) = 2\int (\boldsymbol{\omega}(\boldsymbol{y}) - \boldsymbol{\omega}(\boldsymbol{x}))\,\eta_\sigma(\boldsymbol{x}-\boldsymbol{y})d\boldsymbol{y} \tag{2}$$

To verify the new implementation, the leapfrogging vortex rings test case for `DUST v0.9.0` rVPM formulation are reported in 1. For the initial one-and-a-half leapfrogging cycles, the rVPM curves lie remarkably closer to those of the high-resolution LBM simulation performed by Cheng et al. (Ref. 24). This may prove a greater physical meaningfulness of the reformulated vortex stretching estimation. Besides the initial, ordered leapfrogging, special care should also be put on interpreting the breakdown of the toroidal structures, which, even in this case, takes place after a limited number of cycles, in line with the outcome of the LBM simulation, yet slightly delayed. Interestingly, the gradual loss of coherence appears to be quite synchronized with that obtained by FlowVPM rVPM with Subfilter turbulence model, performed with a much finer discretization (600k particles, against the 56.7k used in `DUST`). The same simulation, performed by the author without SFS contributions, did not manage to predict the vortex structures' turbulent breakdown. Alvarez attributes the ring disruption to the insurgence of turbulent effects, which, in the author's case, do not appear if the SFS models are deactivated. Therefore, the different diffusion scheme (PSE) adopted in the current work appears to somehow introduce such kind of phenomenon itself.

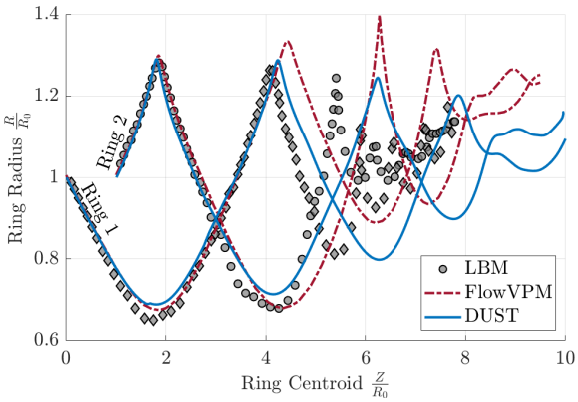

Figure 1: Leapfrogging of vortex rings. Rings radius evolution comparison between `DUST v0.9.0`, Lattice Boltzmann Method (Ref. 24), FlowVPM (Ref. 23)

MODEL DESCRIPTION

A detailed tiltrotor model, representative of the Bell XV-15 research aircraft with Advanced Technology Blades (ATBs) (Ref. 25), has been built in DUST-MBDyn using data published by Acree in Ref. (Ref. 26). The model dynamical model has been presented and validated in (Ref. 27). In contrast, the model has been used in (Ref. 14) to evaluate the trim condition in airplane mode and the unsteady aeroelastic loads during a roll maneuver.

The accuracy and convergence of the aerodynamic mesh are validated by comparing the lift coefficient of the wing-nacelle complex with the experimental results of Fergurson (Ref. 28). The model neglects the presence of the fuselage, which is replaced by the continuation of the wing, and for the vortex lattice mesh, the nacelle is also neglected. The wing span is elongated up the rotor axis to compensate for its effect. In Fig. 2, the lift coefficient curves are compared using a free-stream velocity of $U_\infty = 140$ Knts. The surface panels agree well with the experimental data, while the linear vortex lattice element is estimated to have a loss on lift coefficient of 7%.

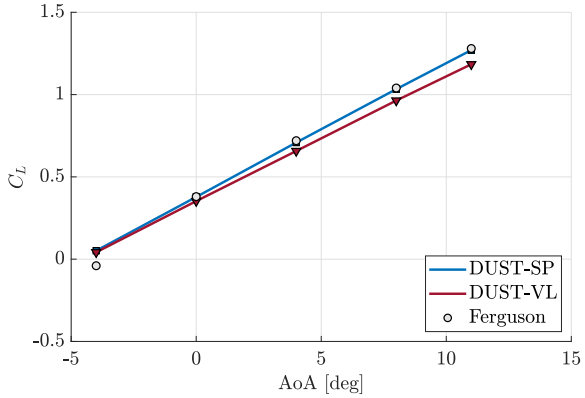

Figure 2: Wing-Nacelle lift coefficient: comparison between the wind tunnel data of Fergurson (Ref. 28) and the surface panel and vortex lattice DUST mesh.

To validate the trim procedure in airplane mode The pitch attitude θ with respect to the flight speed is shown in Fig. 3, compared to similar results obtained in CAMRAD-JA (Ref. 29) which is a suitable reference model since it is based on the aerodynamic characteristics provided by Ferguson in Ref. (Ref. 28), obtained from wind tunnel tests and flight test data. The dashed red curve refers to the model with hybrid aerodynamics (DUST for what concerns the airframe, and MBDyn with dynamic inflow to account for the aerodynamic of the rotors), *i.e.*, *Model A*. In contrast, the blue square markers refer to the model with full DUST aerodynamics, that is, *Model B*. Both models provide similar results to the CAMRAD-JA reference model. At low speeds, on the other hand, it was found a marked deviation from the reference trim curves which is reduced by inserting an aerobody element representing the static aerodynamics of the fuselage in the MBDyn model, based on the aerodynamic lookup tables provided in

Ref. (Ref. 28).

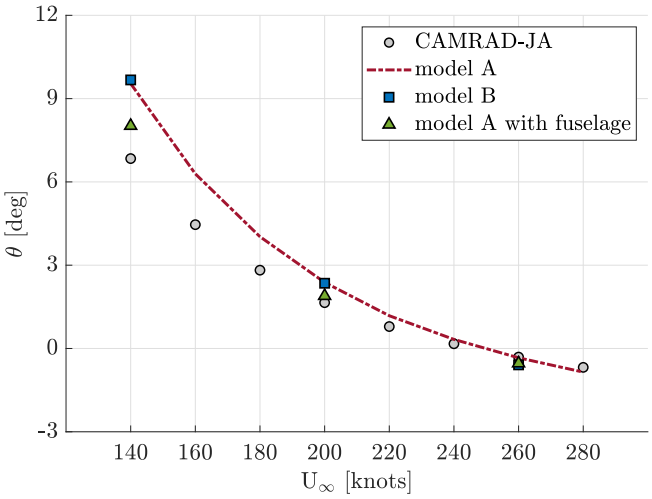

Figure 3: Airframe pitch attitude θ with reference to the flight speed.

The hover predictions for the XV-15 rotor are reported in 4. A comparison is provided between `DUST v0.8.2`, and the current `DUST v0.9.0` with reformulated VPM and the experimental data (run 44) gathered in 1984 at the NASA Outdoor Aeronautical Research Facility (OARF) on a full scale XV-15 proprotor endowed with the aforementioned Advanced Technology Blade (ATB), and reported by Harris (Ref. 30). As shown in fig. 4, the thrust coefficient is better captured from the latest version at collective angles closer to the trim condition, namely, ranging from $\theta_{075} = 10$ deg to $\theta_{075} = 15$ deg.

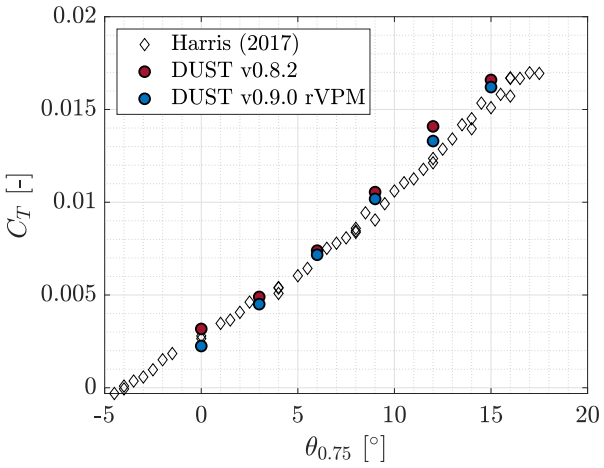

Figure 4: XV-15 rotor with ATB blades, hover validation. Comparison between `DUST v0.8.2`, `DUST v0.9.0` rVPM and the experimental (Ref. 30)

TRANSITION MANEUVER

FLIGHT CONTROL LAWS

To simulate a complete transition maneuver, a Nonlinear Dynamic Inversion (NDI) control law is implemented based on the linearized dynamics of the tiltrotor flight dynamics. Application of NDI control laws to rotorcraft can be found in Refs. 31–44. A key aspect of DI is the reliance on model inversion to cancel the plant dynamics and track a desired reference model. One convenient feature of NDI is that it inverts the plant model in its feedback linearization loop, which, compared to other more conventional model-following control strategies such as explicit model following (EMF), eliminates the need for gain scheduling. However, the plant model used for feedback linearization still needs to be scheduled with the flight condition. A generic DI controller as applied to a linear system is shown in Fig. 5. The key components are a command model (also known as command filter or reference model) that specifies the desired response to pilot commands, a feedback compensation on the tracking error, and an inner feedback loop that achieves model inversion (*i.e.*, the feedback linearization loop).

A multi-loop NDI control law based on Refs. 33, 34, 37, 38, 45 is designed to enable autonomous flight in low-speed flight (helicopter mode), cruise flight (airplane mode), and transition between the two. The schematic of the closed-loop rotorcraft dynamics is shown in Fig. 6. The outer loop controller, shown in Fig. 7b tracks longitudinal, lateral, and vertical ground velocities commands in the heading frame and calculates the desired pitch and roll attitudes for the inner loop to track, in addition to the collective control input setting. The desired response type for the outer loop is Translational Rate Command (TRC). The inner loop, shown in Fig. 7a achieves stability, disturbance rejection, and desired response characteristics about the roll, pitch, yaw, and heave axes. When coupled with the outer loop, an Attitude Command / Attitude Hold (ACAH) response is used for the roll and pitch axes, whereas Rate Command / Attitude Hold (RCAH) is used for the yaw axis.

The objective of the outer-velocity loop is to track longitudinal and lateral velocities in the heading frame. The heading frame is a vehicle-carried frame where the x-axis is aligned with the current aircraft heading, the z-axis is positive up in the inertial frame, and the y-axis points to the right, forming a left-handed orthogonal coordinate system. The following equation shows the rotation from the body to the heading frame:

$$\boldsymbol{T}_{B\to h} = \begin{bmatrix} \cos\theta & \sin\phi\sin\theta & \cos\phi\sin\theta \\ 0 & \cos\phi & -\sin\phi \\ \sin\theta & -\sin\phi\cos\theta & -\cos\phi\cos\theta \end{bmatrix} \tag{3}$$

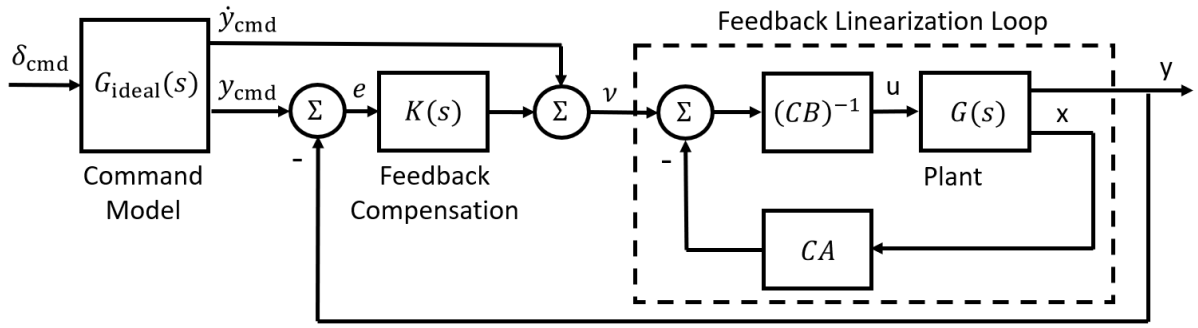

Figure 5: DI controller as applied to a linear system.

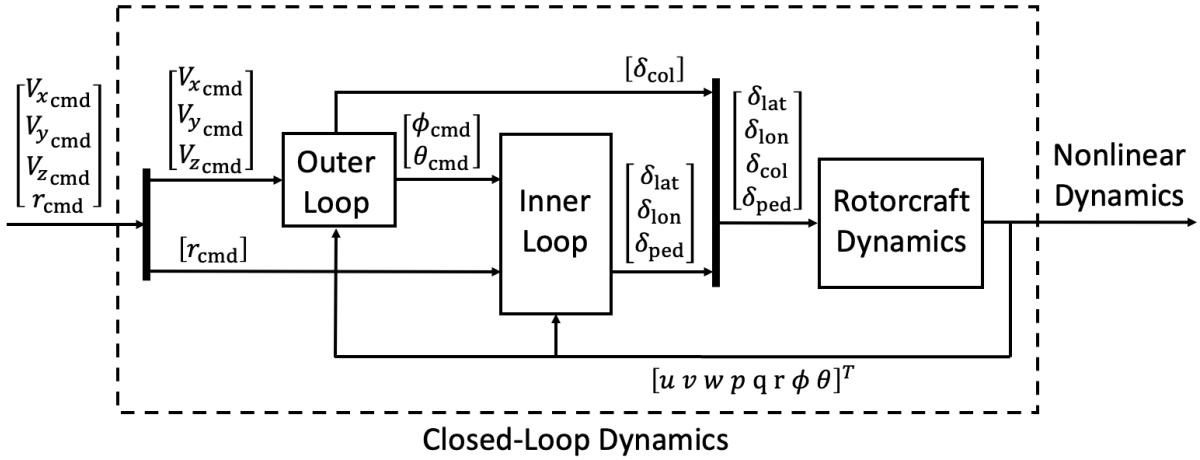

Figure 6: Schematic of the closed-loop tilt-rotor/wing dynamics.

such that the velocities in the heading frame are given by:

$$\begin{bmatrix} V_x \\ V_y \\ V_z \end{bmatrix} = \boldsymbol{T}_{B\to h} \begin{bmatrix} u \\ v \\ w \end{bmatrix} \tag{4}$$

The outer-velocity loop is modified with respect to Ref. 33 not to include the auxiliary control input (*i.e.*, the nacelle angle in the case of tilt-rotor) as a control variable. Rather, the nacelle/wing angle is prescribed with flight speed based on (Ref. 46), but can still be changed via open-loop pilot inputs. The outer loop dynamics are designed based on the following reduced-order dynamics:

$$\begin{bmatrix} \dot{u} \\ \dot{v} \\ \dot{w} \end{bmatrix} = \begin{bmatrix} X_u & 0 & 0 \\ 0 & Y_z & 0 \\ 0 & 0 & Z_w \end{bmatrix} \begin{bmatrix} u \\ v \\ w \end{bmatrix} + \begin{bmatrix} 0 & X_\theta & X_{\delta_{\text{col}}} \\ Y_{\delta_\phi} & 0 & 0 \\ 0 & Z_\theta & Z_{\delta_{\text{col}}} \end{bmatrix} \begin{bmatrix} \phi_{\text{cmd}} \\ \theta_{\text{cmd}} \\ \delta_{\text{col}} \end{bmatrix} \tag{5a}$$

$$\begin{bmatrix} V_x \\ V_y \\ V_z \end{bmatrix} = \begin{bmatrix} \cos\theta_0 & 0 & \sin\theta_0 \\ 0 & 1 & 0 \\ -\sin\theta_0 & 0 & \cos\theta_0 \end{bmatrix} \begin{bmatrix} u \\ v \\ w \end{bmatrix} \tag{5b}$$

where:

- $\boldsymbol{x}$, $\boldsymbol{u}$ are the reduced-order state, control input, and output vectors used for outer-loop control design,
- u, v, w are the longitudinal, lateral, and vertical velocities in the body-fixed frame,
- V_x, V_y, V_z are the longitudinal, lateral, and vertical velocities in the heading frame,
- ϕ_{cmd}, θ_{cmd} are the roll and pitch attitudes commanded to the inner loop,
- X_u, Y_v, Z_W, X_θ, Y_{δ_ϕ}, Z_θ are stability derivatives,
- $X_{\delta_{\text{col}}}$, $Z_{\delta_{\text{col}}}$ are stability derivatives,
- θ_0 is the trim pitch attitude.

Note that the stability and control derivatives are a function of the total speed $V = \sqrt{u^2+v^2+w^2}$, such that the reduced-order dynamics used for flight control design of both inner and outer loops are a function of total speed as well. For this reason, from a practical standpoint, these matrices are computed offline at incremental longitudinal speeds from hover to

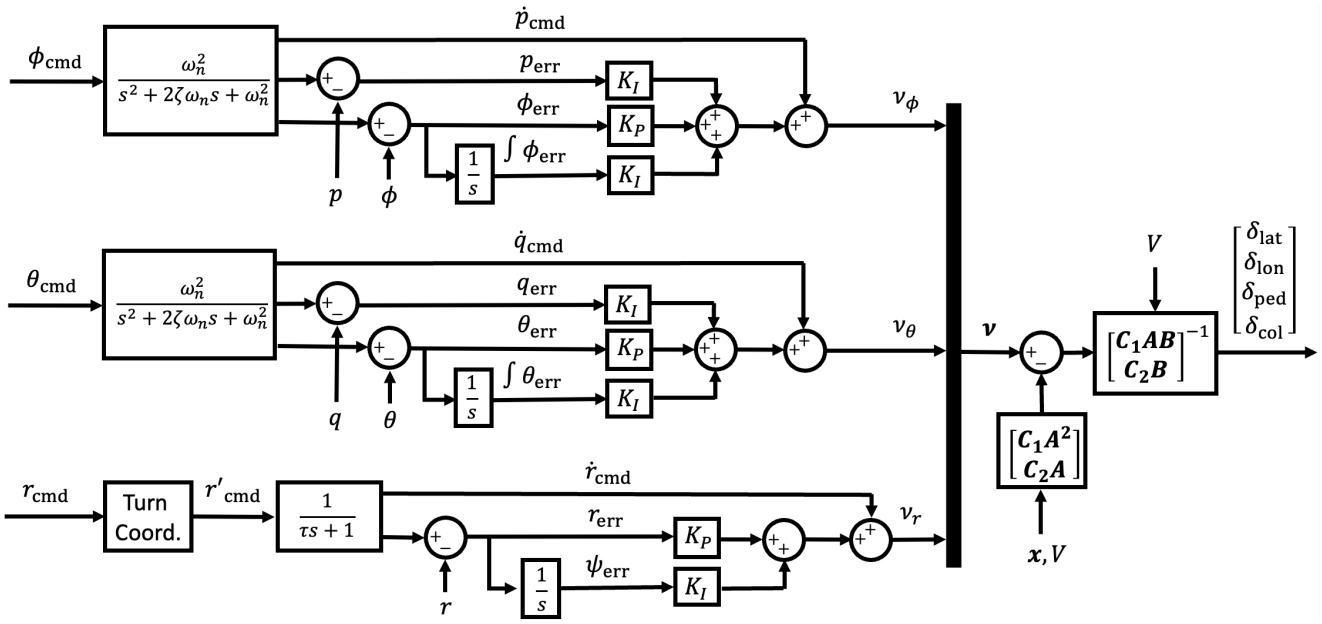

(a) Inner-attitude control loop.

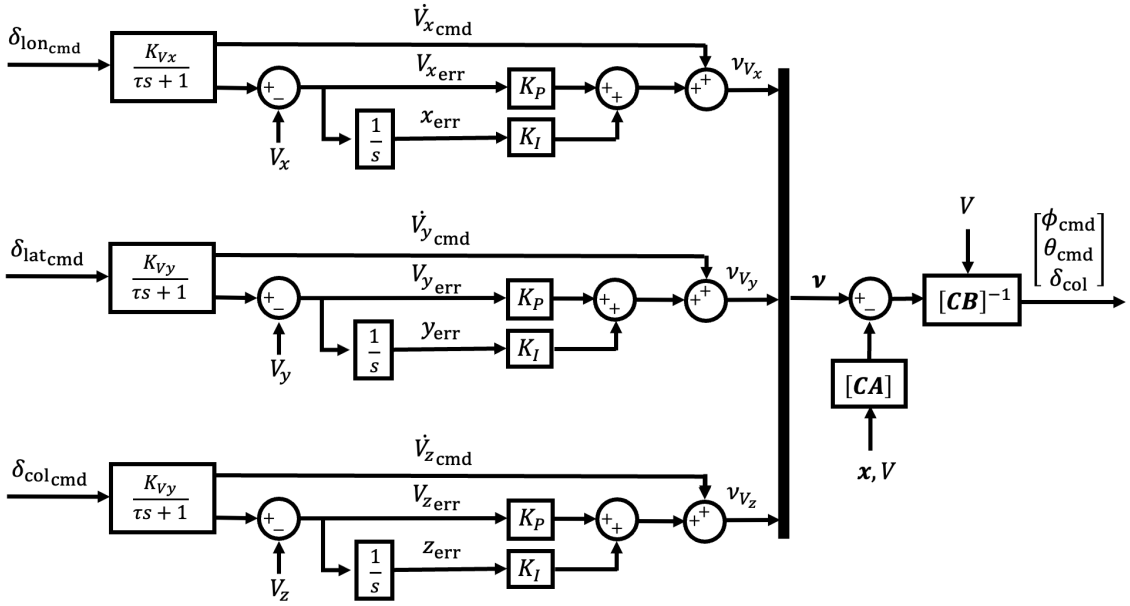

(b) Outer-velocity control loop.

Figure 7: Dynamic inversion inner-attitude and outer-velocity control loops.

the maximum aircraft speed at 20 kts intervals and stored. When the linearized DI controller is implemented on the nonlinear aircraft dynamics, the coefficient matrices are computed at each time step via interpolation based on the current airspeed $V(t)$ and on the lookup tables stored offline. It is important to note that what is implemented in the nonlinear aircraft dynamics is linearized DI. However, because the coefficient matrices are scheduled with the longitudinal speed, and scheduling effectively introduces a nonlinear relation between the aircraft states and the feedback control input, the controller implemented is effectively nonlinear DI (NDI) (Ref. 45). The stability and control derivatives are obtained via the MATLAB®/Simulink generic tiltrotor simulation model described in Ref. 37.

CLOSED-LOOP TRANSITION

The tiltrotor flight dynamics are linearized and residualized at each discreet speed increment to obtain the NDI control law coefficient matrices. Dynamic inversion control laws are demonstrated for closed-loop simulations of acceleration from 80 to 160 kts over 40 seconds, which includes a transition from helicopter to airplane mode. This simulation makes use of the nonlinear rotorcraft dynamics. Figure 8a shows the heading-frame velocities. In this figure, the longitudinal speed is shown to track accurately the reference trajectory, while the off-axis responses in lateral and vertical speed are minimal. Figure 8b shows how the inner-attitude loop is able to track the desired pitch attitude while maintaining zero roll and yaw attitudes. The pitch attitude first decreases to direct the rotor thrust forward and thus accelerates, and then gradually increases as the aircraft reaches a steady acceleration. Finally, Fig. 8c shows the closed-loop control inputs.

RESULTS

In the following section, the rotor loads during the transition will be discussed by comparing two different simulations: the first has been conducted using the MBDyn build-in Pitt-Peters dynamic inflow model for the rotor and a 2D strip theory model for the fixed-wing, whereas the second model relies on the DUST viscous vortex particle model. The structural model for both simulations was the same XV-15 MBDyn model equipped with flexible blades, a drive train model, and a rigid airframe. The choice of having a rigid airframe model was dictated by the fact that aircraft motion is imposed with the results obtained from the simplified XV-15 MATLAB model, and therefore, having a flexible airframe model (representative of the real XV-15) leads to a dynamic behavior that is too flexible since the model is tuned in free-free condition, but, when the motion is imposed, the model is indeed clamped. Instead, a simple governor has been implemented in MBDyn for the rotor. By changing the collective, the goal was to maintain the rotor speed at 601 rpm with a constant torque of 1100 hp for the entire transition maneuver. The two simulations were carried out using a machine equipped with Intel(R) Core(TM) i9-10980XE with 18 physical cores and an NVIDIA A4000 GPU employed to compute the flowfield of fig. 11. In total, the first simulation took 15 minutes to compute, whereas the coupled simulation took 48 hours using a time step of 0.001 sec, corresponding to 100 steps per rotor revolution.

LOADS COMPARISON

In fig. 9 and fig. 10 present samples of the loads that can be extracted from the simulations for two different nacelle angles: 90 and 60 degrees since, in these conditions, the rotor internal forces are higher. fig. 9a and fig. 10a show the blade deformation averaged over one rotor revolution: MBDyn alone and the coupled simulation agree. At 90 deg, the flap component shows an almost rigid deformation due mainly to the high gimbal angles (fig. 9b) that arise when the wind speed is particularly high (80 kts), and the nacelle is still at 90 deg. In particular, the coupled simulation reaches a maximum gimbal angle of 12 deg, which is over the allowed limits of 10 deg: this suggests the need to implement a flapping control that limits gimbal angles. Regarding the blade's internal moments, both simulations show similar behavior, particularly for the flapping component, although the coupled simulation predicts loads that are, on average, higher (fig. 10d. Finally, regarding the wing moments in helicopter mode (fig. 9e, the torsion moment appears to be the highest: in particular, the coupled simulation predicts a significant variation of this moment at 3/rev. This can be explained by the fact that the coupled simulation captures the aerodynamic interaction between the wing and rotor. At 60 deg (fig. 10e), the chordwise moment is the one with the greatest oscillation: in this case, the MBDyn alone simulation predicts larger oscillation with respect to the coupled simulation. This can be explained by the fact that, in this case, the gimbal angles are greater in the MBDyn alone simulation, and therefore, the loads transmitted to the fixed airframe are larger.

FLOWFIELD VISUALIZATION

Figure 11 shows the wake evolution of the tiltrotor during the conversion maneuver. The wake is visualized using isovorticity surfaces colored by the normalized velocity. In helicopter mode, the rotor wake is characterized by strong tip vortexes that are broken after 4-5 revolutions into smaller vortexes in an almost turbulent flow. As the wind increases and the nacelle continues to rotate, the rotor wake becomes more and more helicoidal; in particular, this ordered shape is clearly visible from 45 deg up to 0 deg. Moreover, as the wind increases, the wake is stretched out, and the tip vortex becomes less intense.

CONCLUSION

This work investigates the aeromechanics of tiltrotor conversion maneuver using the multibody code MBDyn coupled with the mid-fidelity aerodynamic code DUST. The analytical model is based on the XV-15, which has advanced technology blades in size and dynamic characteristics. The hover and cruise performance of the present XV-15 analytical model is validated against available test data. A generic tiltrotor control system is developed using a non-linear dynamic inversion control law to simulate transient conversion maneuvers. Time histories of vehicle dynamics, rotor controls, rotor flapping, rotor performance, and blade structural loads are investigated. The following conclusion can be obtained:

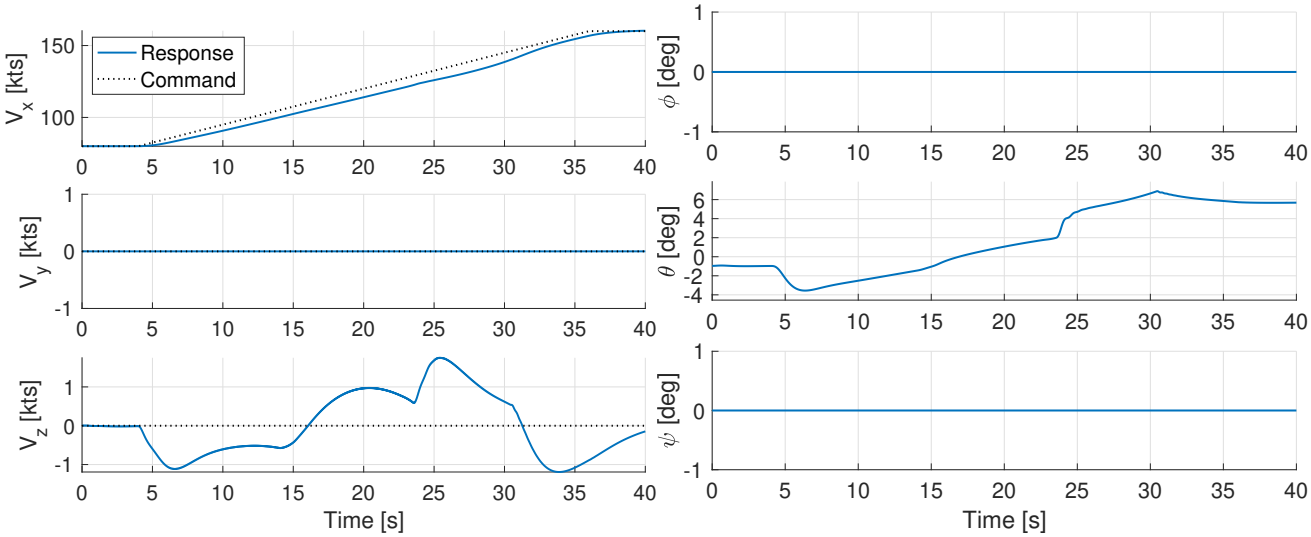

(a) Heading-frame velocities.

(b) Euler angles.

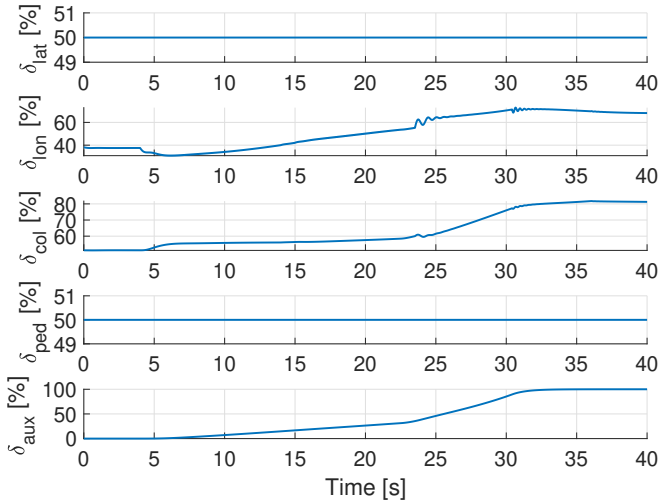

(c) Control inputs.

Figure 8: Autonomous transition from 80 kts (helicopter mode) to 160 kts (airplane mode).

1. The calculations of rotor and airframe performance are in reasonably good agreement with the available XV-15 test data for both hover thrust sweep and cruise speed sweep when adopting the vortex particle aerodynamic model.

2. The actual aircraft airspeed is followed very well by the controller, and the altitude is well maintained.

3. The loads comparison between the MBDyn model and the coupled model are in overall agreement, in particular when considering the rotor loads. The differences become more significant when considering the internal forces on the wing since the MBDyn alone model cannot capture rotor-wing interactions.

In future work, the controller will be embedded in the simulation in order to have a tight coupling between the mid-fidelity model and the controller. Moreover, a GPU implementation of DUST could lead to a speed-up of this simulation of almost 10 times, allowing the possibility to easily investigate different control strategies and conversion profiles.

REFERENCES

1. Maisel, M. D., Giulianetti, D. J., and Dugan, D. C., *The History of The XV-15 Tilt Rotor Research Aircraft - From Concept to Flight*, National Aeronautics and Space Administration, Office of Policy and Plans . . . , NASA SP-2000-4517, Monographs in Aerospace History #17, 2000.

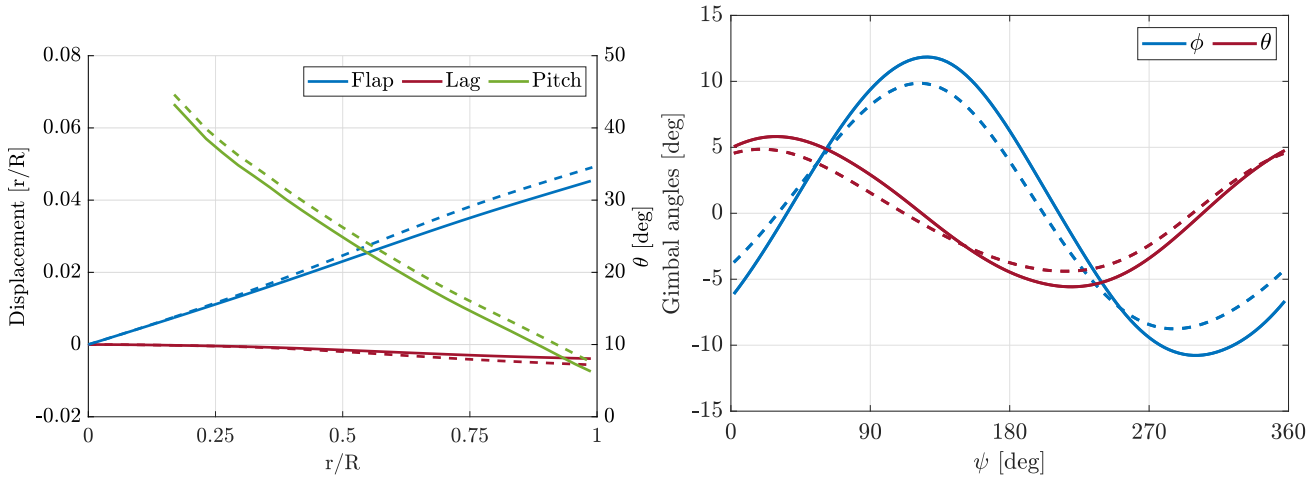

(a) Blade deformation

(b) Gimbal angles

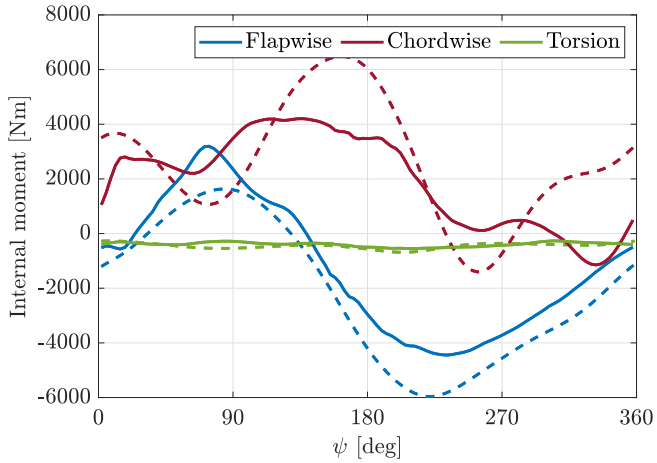

(c) Blade internal moments at 0.25% R

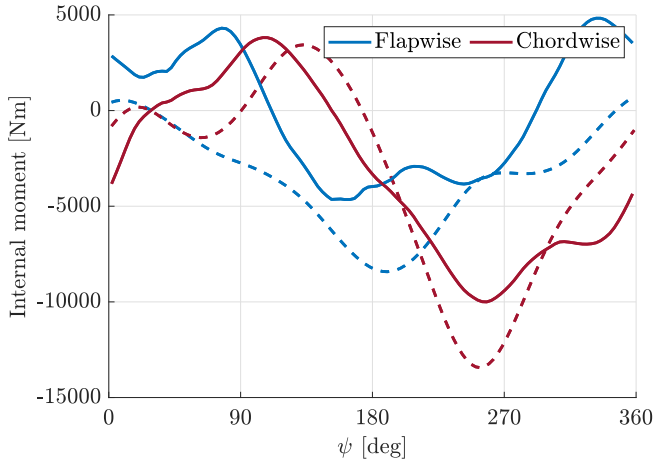

(d) Blade internal moments at 0.1% R

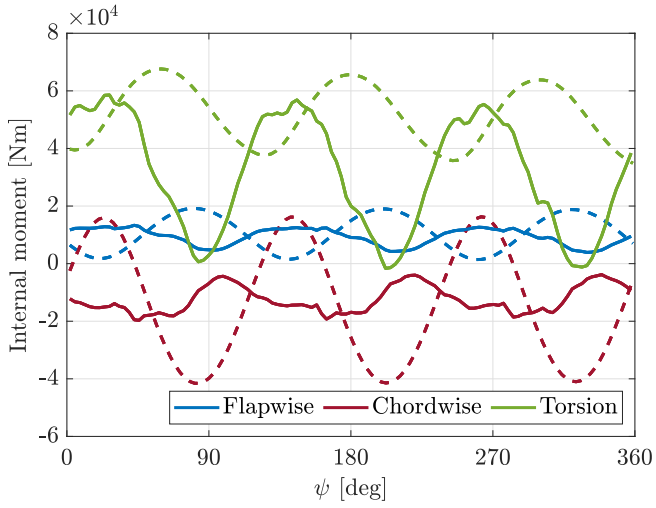

(e) Wing internal moment at the root

Figure 9: XV-15 sample loads for θ_{nacelle} = 90 deg. Continuous lines: DUST-MBDyn model, dashed lines: MBDyn alone model

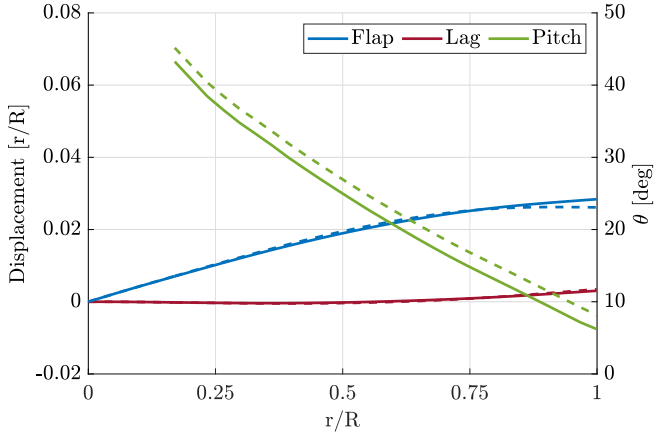

(a) Blade deformation

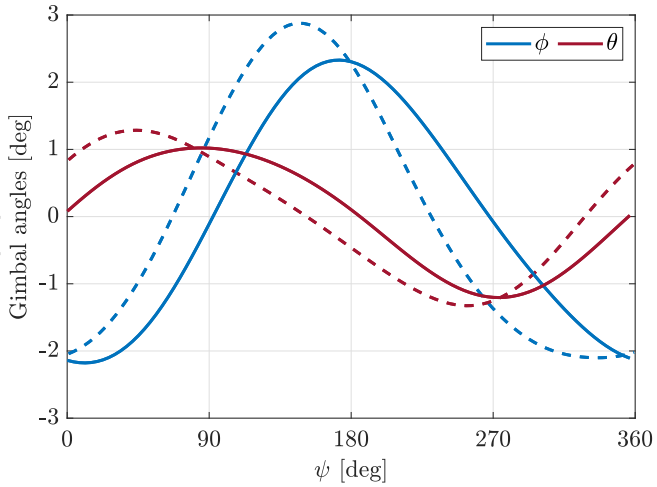

(b) Gimbal angles

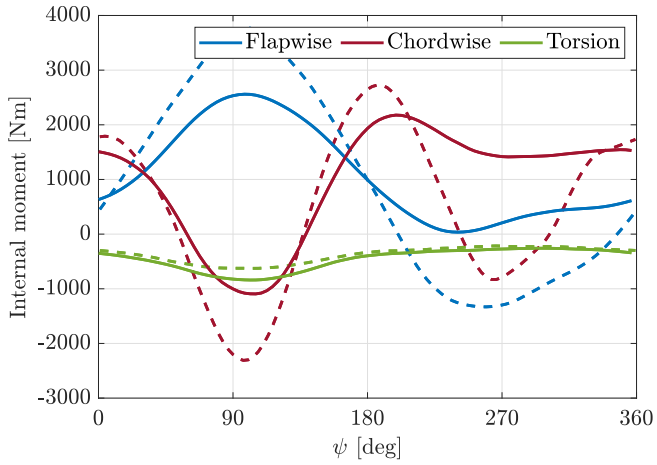

(c) Blade internal moments at 0.25% R

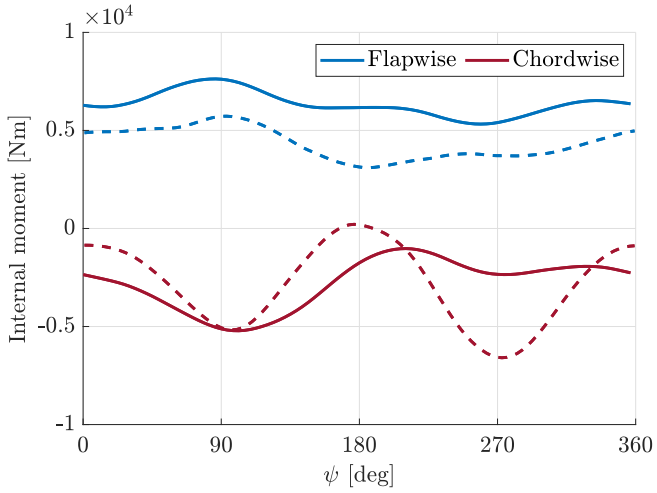

(d) Blade internal moments at 0.1% R

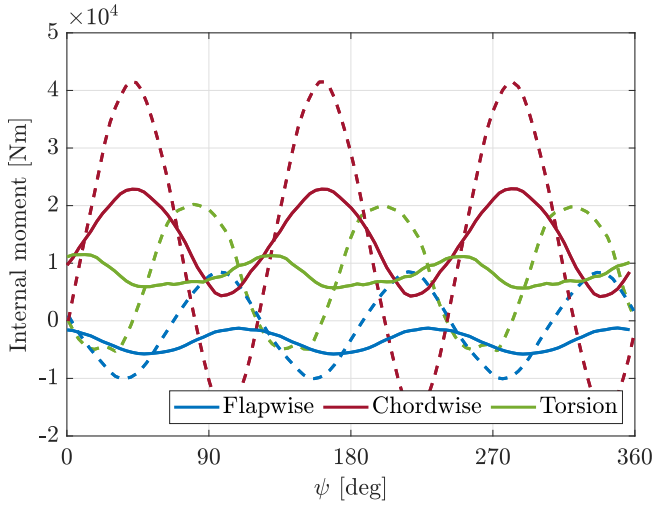

(e) Wing internal moment at the root

Figure 10: θ_{nacelle} = 60 deg. Continuous lines: DUST-MBDyn model, dashed lines: MBDyn alone model

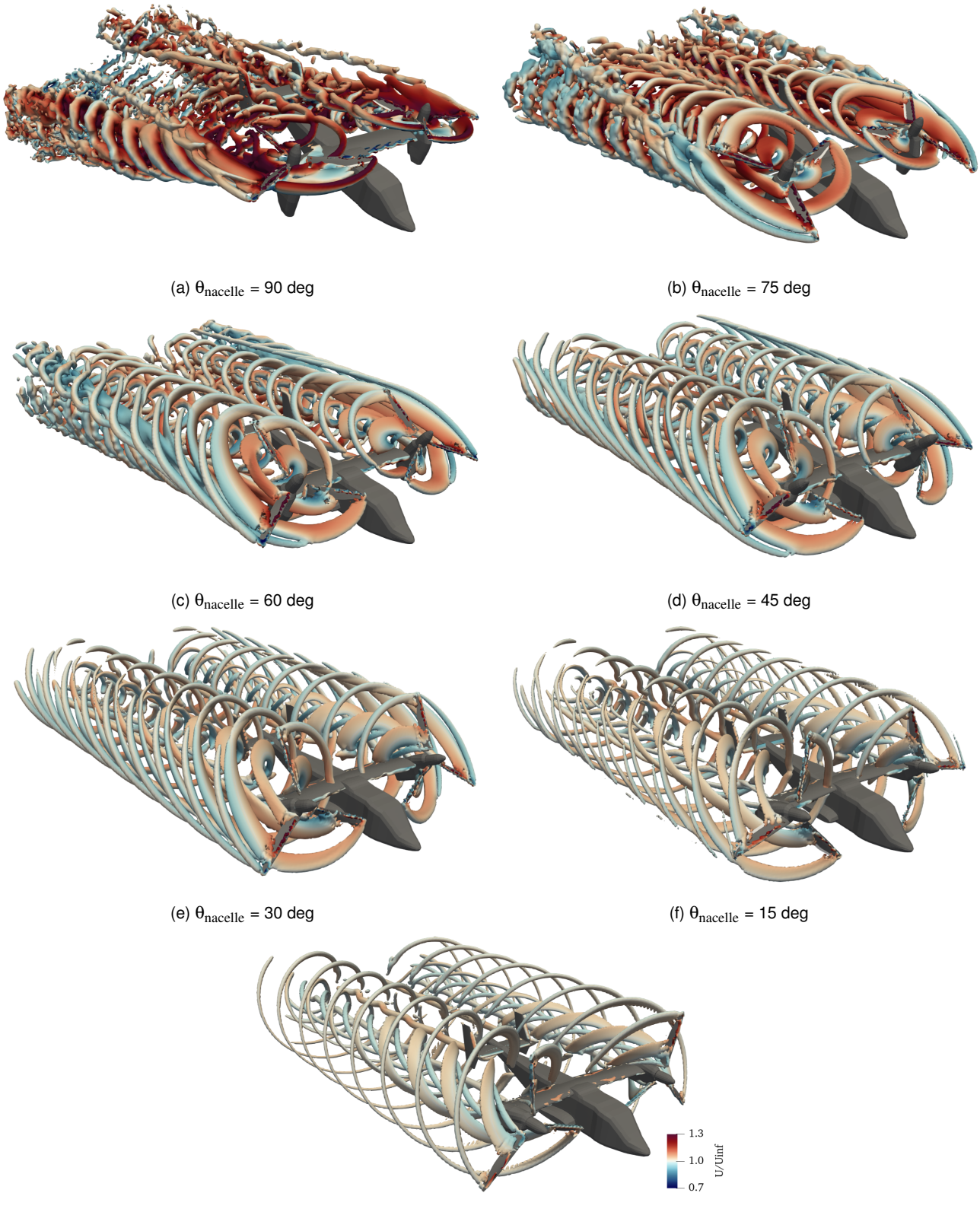

(a) θ_{nacelle} = 90 deg

(b) θ_{nacelle} = 75 deg

(c) θ_{nacelle} = 60 deg

(d) θ_{nacelle} = 45 deg

(e) θ_{nacelle} = 30 deg

(f) θ_{nacelle} = 15 deg

(g) θ_{nacelle} = 0 deg

Figure 11: Wake visualization of the coupled DUST-MBDyn simulation by means of isovorticity contour $(Q = 100)$ colored by the adimensionalized velocity U/U_∞

2. Deckert, W. H., and Ferry, R. G., “Limited Flight Evaluation of the XV-3 Aircraft,” Report AFFTC-TR-60-4, Air Force Flight Test Center, May 1960.

3. Rosenstein, H., and Clark, R., “Aerodynamic Development of the V-22 Tilt Rotor,” 12th European Rotorcraft Forum, September 22-25 1986.

4. Ehinger, R., Gehler, C., and Allen, S., “Bell V-280 Valor: A JMR-TD Program Update,” Proceedings of the 73rd Annual Forum of the American Helicopter Society, May 9–11 2017.

5. Parham, T., Jr., and Corso, L. M., “Aeroelastic and Aeroservoelastic Stability of the BA 609,” 25th European Rotorcraft Forum, September 14–16 1999.

6. Fraser, W., King, D., Schaeffer, J. M., and Wells, D., “Development of Powered-Lift Airworthiness Standards as Applied to the AW609 Tiltrotor Certification Basis,” Proceedings of the 74th Annual Forum of the American Helicopter Society, May 14–17 2018.

7. ACARE — Report of the Group of Personalities, “European Aeronautics: a Vision for 2020,” , January 2001.

8. Tran, S. A., and Yeo, H., “Transient and Quasi-steady Numerical Simulations of Tiltrotor Conversion Maneuvers,” *Journal of the American Helicopter Society*, Vol. 68, (2), 2023, pp. 18–32.

9. Saberi, H., Khoshlahjeh, M., Ormiston, R. A., and Rutkowski, M. J., “Overview of RCAS and application to advanced rotorcraft problems,” American helicopter society 4th decennial specialists’ conference on aeromechanics, San Francisco, CA, 2004.

10. Wissink, A. M., Jude, D., Jayaraman, B., Roget, B., Lakshminarayan, V. K., Sitaraman, J., Bauer, A. C., Forsythe, J. R., and Trigg, R. D., “New capabilities in CREATE-AV helios version 11,” AIAA Scitech 2021 Forum, 2021.

11. Savino, A., Cocco, A., Zanotti, A., Tugnoli, M., Masarati, P., and Muscarello, V., “Coupling Mid-Fidelity Aerodynamics and Multibody Dynamics for the Aeroelastic Analysis of Rotary-Wing Vehicles,” *Energies*, Vol. 14, (21), 2021, pp. 6979.

12. Tugnoli, M., Montagnani, D., Syal, M., Droandi, G., and Zanotti, A., “Mid-fidelity approach to aerodynamic simulations of unconventional VTOL aircraft configurations,” *Aerospace Science and Technology*, Vol. 115, 2021, pp. 106804. DOI: https://doi.org/10.1016/j.ast.2021.106804.

13. Masarati, P., Morandini, M., and Mantegazza, P., “An Efficient Formulation for General-Purpose Multibody/Multiphysics Analysis,” *Journal of Computational and Nonlinear Dynamics*, Vol. 9, (4), 07 2014.

14. Savino, A., Cocco, A., and Muscarello, V., “Evaluation of dynamic loads and performance indexes in tiltrotors using a mid-fidelity aeroservoelastic tool,” *Aerospace Science and Technology*, 2024, pp. 108929.

15. Cocco, A., and Savino, A., “Tiltrotor Whirl-Flutter Assessment by Multifidelity Aerodynamic Models,” AIAA Scitech 2024 Forum, 2024.

16. Zanotti, A., Savino, A., Palazzi, M., Tugnoli, M., and Muscarello, V., “Assessment of a Mid-Fidelity Numerical Approach for the Investigation of Tiltrotor Aerodynamics,” *Applied Sciences*, Vol. 11, (8), 2021, pp. 3385.

17. Masarati, P., and Morandini, M., “Intrinsic Deformable Joints,” *Multibody System Dynamics*, Vol. 23, (4), doi:10.1007/s11044-010-9194-y, 2010, pp. 361–386.

18. Ghiringhelli, G. L., Masarati, P., and Mantegazza, P., “A Multi-Body Implementation of Finite Volume C^0 Beams,” *AIAA Journal*, Vol. 38, (1), doi:10.2514/2.933, January 2000, pp. 131–138.

19. Morandini, M., and Masarati, P., “Implementation and Validation of a 4-Node Shell Finite Element,” ASME IDETC/CIE 2014, DETC2014-34473, August 17–20 2014.

20. Craig, R. R., Jr., and Bampton, M. C. C., “Coupling of Substructures for Dynamic Analysis,” *AIAA Journal*, Vol. 6, (7), doi:10.2514/3.4741, July 1968, pp. 1313–1319.

21. Bungartz, H.-J., Lindner, F., Gatzhammer, B., Mehl, M., Scheufele, K., Shukaev, A., and Uekermann, B., “preCICE – A fully parallel library for multi-physics surface coupling,” *Computers and Fluids*, Vol. 141, Advances in Fluid-Structure Interaction, 2016, pp. 250–258. DOI: https://doi.org/10.1016/j.compfluid.2016.04.003.

22. Goland, M., “The flutter of a uniform cantilever wing,” *Journal of Applied Mechanics-Transactions of the Asme*, Vol. 12, (4), 1945, pp. A197–A208.

23. Alvarez, E., and Ning, A., “Development of a Vortex Particle Code for the Modeling of Wake Interaction in Distributed Propulsion,” AIAA Applied Aerodynamics Conference, Atlanta, GA, 06 2018. DOI: 10.2514/6.2018-3646.

24. Cheng, M., Lou, J., and Lim, T., “Leapfrogging of multiple coaxial viscous vortex rings,” *Physics of Fluids*, Vol. 27, (3), 2015.

25. Maisel, M., "NASA/Army XV-15 Tilt-Rotor Research Aircraft Familiarization Document," TM X-62,407, NASA, January 1975.

26. C. W. Acree, J., "An Improved CAMRAD Model for Aeroelastic Stability Analysis of the XV-15 With Advanced Technology Blades," TM 4448, NASA, 1993.

27. Cocco, A., Savino, A., and Masarati, P., "Flexible Multibody Model of a Complete Tiltrotor for Aeroservoelastic Analysis," ASME IDETC/CIE 2022, doi:10.1115/DETC2022-88973, August 14–17 2022.

28. Ferguson, S. W., Clement, W. F., Cleveland, W. B., and Key, D. L., "Assessment of simulation fidelity using measurements of piloting technique in flight," American Helicopter Society 40th Annual Forum, May 16–18 1984.

29. Muscarello, V., and Quaranta, G., "Structural Coupling and Whirl-Flutter Stability with Pilot-in-the-Loop," *Journal of the American Helicopter Society*, Vol. 66, (3), 2021, pp. 1–16.

30. Harris, F., "Hover performance of isolated proprotors and propellers - Experimental data," Technical report, 2017.

31. Saetti, U., Horn, J. F., Lakhmani, S., Lagoa, C., and Berger, T., "Design of Dynamic Inversion and Explicit Model Following Control Laws for Quadrotor UAS," *Journal of the American Helicopter Society*, **65**, 032006 (2020). DOI: https://doi.org/10.4050/JAHS.65.032006.

32. Saetti, U., Enciu, J., and Horn, J. F., "Flight Dynamics and Control of an eVTOL Concept Aircraft with a Propeller-Driven Rotor," *Journal of the American Helicopter Society*, **67**, 032012 (2022). DOI: https://doi.org/10.4050/JAHS.67.032012.

33. Berger, T., Tischler, M. B., and Horn, J. F., "Outer-Loop Control Design and Simulation Handling Qualities Assessment for a Coaxial-Compound Helicopter and Tiltrotor," Proceedings of the 77th Annual Forum of the Vertical Flight Society, Virtual, Oct 5-8, 2020.

34. Berger, T., Tischler, M. B., and Horn, J. F., "High-Speed Rotorcraft Pitch Axis Response Type Investigation," Proceedings of the 77th Annual Forum of the Vertical Flight Society, Virtual, May 10-14, 2021.

35. Saetti, U., Horn, J. F., and Berger, T., "On the effects of rotor induced vibrational stability on helicopter flight dynamics," *CEAS Aeronautical Journal,* Article in Advance, 2024. DOI: https://doi.org/10.1007/s13272-024-00718-w.

36. Saetti, U., Rogers, J. D., Alam, M., and Jump, M., "Tau Theory-Based Flare Control in Autonomous Helicopter Autorotation," *Aerospace*, Vol. 11, (1), 2024. DOI: https://doi.org/10.3390/aerospace11010033.

37. Saetti, U., and Bugday, B., "Tiltrotor Simulations with Coupled Flight Dynamics, State-Space Aeromechanics, and Aeroacoustics," *Journal of the American Helicopter Society*, Vol. 69, (1), 2024. DOI: https://doi.org/10.4050/JAHS.69.012003.

38. Saetti, U., and Guner, F., "Interactional Aerodynamics Modeling and Flight Control Design of Multi-Rotor Aircraft," Proceedings of the 6th Decennial Aeromechanics Specialits' Conference, Santa Clara, CA, Feb 6–8, 2024.

39. Sahani, N. A., and Horn, J. F., "Adaptive Model Inversion Control of a Helicopter with Structural Load Limiting," *Journal of Guidance, Control, and Dynamics*, Vol. 29, (2), 2006, pp. 411–420. DOI: https://doi.org/10.2514/1.13391.

40. Theron, J. P., Horn, J. F., Wachspress, D. A., and Enciu, J., "Nonlinear dynamic inversion control for urban air mobility aircraft with distributed electric propulsion," Proceedings of the 76th Annual Forum of the Vertical Flight Society, October 5–8, 2020. DOI: https://doi.org/10.4050/F-0076-2020-16396.

41. Walter, A., Mckay, M., Niemiec, R., Gandhi, F., and Berger, T., "Hover Dynamics and Flight Control of a UAM-Scale Quadcopter With Hybrid RPM and Collective Pitch Control," *Journal of the American Helicopter Society*, **68**, 022012 (2023), pp. 143–160(18). DOI: https://doi.org/10.4050/JAHS.68.022012.

42. Enciu, J., Horn, J. F., and Langelaan, J. W., "Formation Control of a Rotorcraft Multilift System," *Journal of the American Helicopter Society*, Vol. 62, (4), 2022, pp. 1–14(14). DOI: https://doi.org/10.4050/JAHS.62.042011.

43. Spires, J. M., and Horn, J. F., "Multi-Input Multi-Output Model-Following Control Design Methods for Rotorcraft," *Journal of the American Helicopter Society*, **66**, 032002 (2021), pp. 1–15(15). DOI: https://doi.org/10.4050/JAHS.66.032002.

44. Scaramal, M., and Horn, J. F., "Load Alleviation on Compound Rotorcraft Using Load Feedback and Extremum Seeking Control," *Journal of Guidance, Control, and Dynamics*, Vol. 46, (12), 2023. DOI: https://doi.org/10.2514/1.G007192.

45. Horn, J. F., "Non-Linear Dynamic Inversion Control Design for Rotorcraft," *Aerospace*, Vol. 6, (38), 2019. DOI: https://doi.org/10.3390/aerospace6030038.

46. Ferguson, S. W., “A Mathematical Model for Real Time Flight Simulation of a Generic Tilt-Rotor Aircraft,” CR 166536, NASA, 1988.